

Rendering Iridescent Colors of Optical Disks

Yinlong Sun, F. David Fracchia, Mark S. Drew, Thomas W. Calvert

School of Computing Science, Simon Fraser University, Burnaby, BC, Canada V5A 1S6

Abstract: Iridescent colors of optical disks are caused by light diffraction from their surface microstructure. This paper proposes a diffractive illumination model for optical disks based on their physical structure and the superposition principle of light waves. This model includes contributions due to diffractive and non-diffractive factors. For the diffractive part, we first model the pit periodicity for optical disks by using identical spheres and then simplify their distribution by uniform groups of spheres. We also propose and prove the condition for highlights on illuminated grooved surfaces; this condition provides the non-diffractive contribution. The rendered images using this model achieve excellent agreement with photographs of real optical disks.

Keywords: iridescent colors, optical disks, diffraction, illumination, spectral rendering.

1 Introduction

Iridescent colors are commonly observed on optical disks such as CD-ROMs and writable CDs. When illuminated by a white light source, an optical disk typically demonstrates a bright rainbow-like strip called the *major strip* across the disk center, and two *minor strips* of weaker intensities whose colors vary from bluish to dark brown in the *transverse* direction (cf. Color Plate 1). The colors and positions of the strips change sensitively with both illuminating and viewing directions.

Recently, Stam [Stam99] pointed out that the iridescent colors are caused by light diffraction and derived the reflectance using Beckmann's solution of electromagnetic scattering on rough surfaces, which approach was previously proposed for developing illumination models [He91]. However, Stam's rendered images of optical disks show *many strips* under a directional light source, which does not agree with the real appearance that a disk typically demonstrates only *one major strip*. Moreover, it is our opinion that Beckmann's solution is not appropriate for the case of optical disks because it requires two conditions: the curvature radius of the boundary surface is much larger than the wavelength and the boundary surface is perfectly conducting (see [Beckmann63], pages 20 and 28). Unfortunately, neither condition necessarily holds for optical disks (see [Sun99] for a detailed discussion).

This paper proposes a new approach to the problem – deriving an illumination model for optical disks based on their physical microstructure and the superposition principle of light waves [Sun99]. This model includes contributions from both diffractive and non-diffractive factors. For the diffractive part, we first model the pit periodicity for optical disks by using identical spheres and then approximate their distribution as uniform groups of spheres. We also propose and prove the condition for highlights on illuminated grooved surfaces, and this condition provides the non-diffractive contribution. The rendering is done completely based on spectral information, to which we apply the *composite model* [Sun99] that represents a spectrum as a smooth background plus a series of spikes. The composite model is accurate, compact and efficient, and is especially capable to handle spectral peaks that are dynamically created by light diffraction. Our rendered images of optical disks closely match the corresponding photographs and achieve good realism.

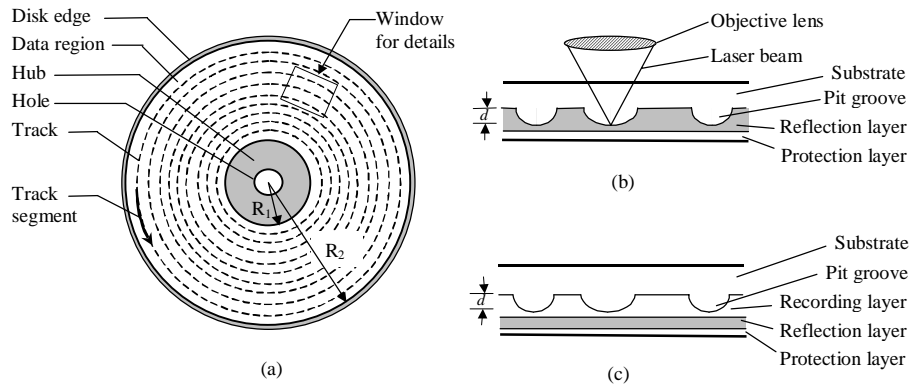


Fig. 1: Physical structure of optical disks: (a) The surface organization. (b) Cross-section of a CD-ROM. (c) Cross-section of a writable CD.

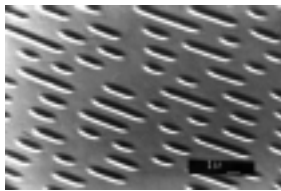


Fig. 2: Photograph of the surface of an optical disk taken with an electron microscope (courtesy of Christian Noldeke) [Noldeke90]. The oval shapes correspond to pit grooves. The track separations and pits widths are uniform, but the lengths and separations of pit grooves are *multiples* of a unit length.

2 Physical Structure and Model

Fig. 1 schematically describes the physical structure of optical disks. The disk surface consists of three regions: the *data region* (between R_1 and R_2), the *hub* (below R_1) and the *disk edge* (above R_2). The data region, which is responsible for the iridescent colors, is structured with pits along concentric tracks, while the hub and disk edge areas are flat. The diagrams in (b) and (c) are cross-sectional views of a CD-ROM and a writable CD along a track segment, e.g. along the curved arrow shown in (a). The multi-layered structure includes a *substrate* (polyvinyl chloride, PMMA or glass), a *reflection layer* (aluminum), and a *protection layer* (lacquer) [Schwartz93]. A writable CD has an additional *recording layer* where pits are burned with laser beams [Purcell97].

Since our goal focuses on rendering the iridescent colors, the most important information is the 2D distribution of pits. Fig. 2 shows an electron microscope photograph [Noldeke90] of a small surface area, as indicated by the rectangular window (exaggerated) in Fig. 1(a). Note that the relative positions of pits are not synchronized amongst different tracks. In other words, given a track, we may regard the start position of a pit as random. The relevant macroscopic and microscopic parameters of CD-ROMs are given in Tables 1 and 2.

Thus we model the hub and disk edge areas as cylinder shells of homogeneous transparent material with smooth surfaces, and the data area as a simple surface (instead of multiple layers) decorated with a partially periodic microstructure.

Table 1: CD ROM's macroscopic parameters. **Table 2:** CD ROM's microscopic parameters

Parameter	Value (mm)
Disk radius	60
Hole radius	7.5
R_1	19
R_2	58.5
Thickness of CD-ROMs	1.1

Parameter	Description	Value (nm)
b	Track spacing	1600
a	Pit length step	300
s	Pit separation	900-3300
l	Pit length	900-3300
w	Pit width	600
d	Pit depth	120

3 Illumination Model

3.1 Diffractive Contribution

For a structure to cause significant diffraction under incoherent lights such as daylight or incandescent lamps, it must satisfy two conditions [Born75, Hecht98]. First, the structure must be periodic or partially periodic. Second, the periodic spacing must be comparable to the wavelengths of light. An optical disk satisfies both conditions.

Consider light diffraction due to a small neighborhood area of point P as shown in Fig. 3(a). We assume that the light source at S and the camera at C are both far away enough from P. Let $\hat{\mathbf{c}}$ and $\hat{\mathbf{t}}$ denote the unit vectors of the radian and track directions for such a neighborhood area (we use hatted symbols to denote unit vectors and bold symbols to denote vectors). Since the size of the shaded rectangle is very small, we can regard $\hat{\mathbf{c}}$ as the direction from the disk center to point O and $\hat{\mathbf{t}}$ as the track direction at point O. Fig. 3(b) shows the coordinate frame constructed for the shaded rectangle, with x , y and z -axes along $\hat{\mathbf{c}}$, $\hat{\mathbf{t}}$, and the disk surface normal, respectively.

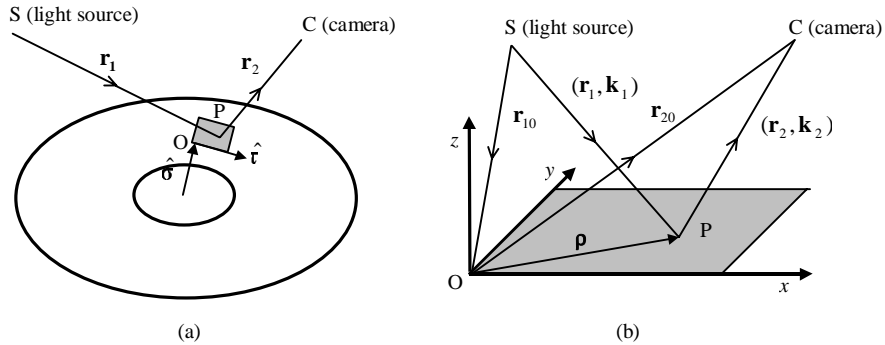


Fig. 3: Constructing the coordinate frame for a small illuminated area.

According to optics, the intensity of a light wave is proportional to the product between light field and its complex conjugate

$$I \propto |E|^2 = E \cdot E^*, \quad (3.1)$$

where E is the light field. For a monochromatic light of wavelength λ , the field can be written as

$$E(\mathbf{r}) = E_0 e^{i\mathbf{k} \cdot \mathbf{r}}, \quad (3.2)$$

where \mathbf{r} is the location, \mathbf{k} is the wave vector ($\mathbf{k} = k\hat{\mathbf{k}}$, with $k = 2\pi/\lambda$ and $\hat{\mathbf{k}}$ the unit

vector along the propagation direction), and E_0 is the amplitude (independent of \mathbf{r} and \mathbf{k}). Thus, the field at the camera location C contributed by the path S-P-C is

$$E(\boldsymbol{\rho}) = E_0 e^{i(\mathbf{k}_1 \cdot \mathbf{r}_1 + \mathbf{k}_2 \cdot \mathbf{r}_2)}, \quad (3.3)$$

where $\boldsymbol{\rho}$ denotes location P in the xy -plane, \mathbf{r}_1 and \mathbf{r}_2 are spatial vectors from S to P and from P to C, and \mathbf{k}_1 and \mathbf{k}_2 are the corresponding wave vectors. From Fig. 3(b), we have $\mathbf{r}_1 = \mathbf{r}_{10} + \boldsymbol{\rho}$ and $\mathbf{r}_2 = \mathbf{r}_{20} - \boldsymbol{\rho}$. Thus

$$E(\boldsymbol{\rho}) = E_0 e^{i(\mathbf{k}_1 \cdot \mathbf{r}_{10} + \mathbf{k}_2 \cdot \mathbf{r}_{20})} \cdot e^{i(\mathbf{k}_1 - \mathbf{k}_2) \cdot \boldsymbol{\rho}} = E'_0 e^{i(\mathbf{k}_1 - \mathbf{k}_2) \cdot \boldsymbol{\rho}} = E'_0 e^{i\mathbf{q} \cdot \boldsymbol{\rho}}, \quad (3.4)$$

where $\mathbf{q} = \mathbf{k}_1 - \mathbf{k}_2$ and E'_0 combines E_0 and the first exponential factor, which is independent of $\boldsymbol{\rho}$. According to the superposition principle, the field at C contributed by the whole shaded rectangle is

$$E = \iint E(\boldsymbol{\rho}) dx dy, \quad (3.5)$$

where the integrals are over the shaded rectangle.

Let us decompose this field as

$$E = E_{\text{track}} + E_{\text{land}}, \quad (3.6)$$

where E_{track} and E_{land} are the contributions from the tracks and the rest area (called the *land area*). Since the land area is flat, it behaves like a mirror and hence merely contributes to the specular reflection. For diffraction we only need to focus on E_{track} .

Our approach is to model a pit groove using identical spheres of diameter a (see Table 2). Fig. 4(a) shows an original layout of pit grooves and (b) is the corresponding representation by our model. A pit groove is thus represented by a group of consecutive shaded spheres and an empty space between two pit grooves in a track is represented with a group of unshaded spheres. In Fig. 4(b), we have also taken into account the staggered distribution of pits among different tracks; that is, the centers of the first spheres (the spheres lying on the y -axis) in different tracks have different unrelated x coordinates.

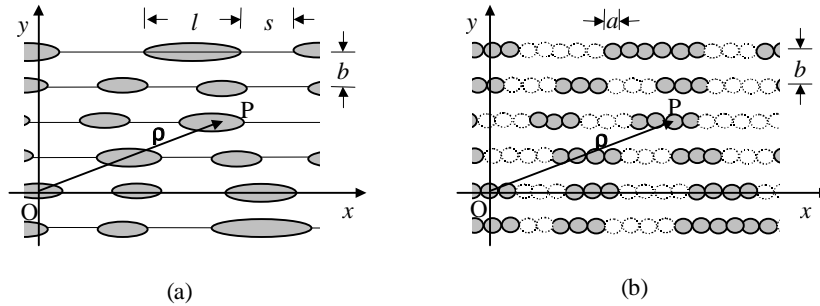


Fig. 4: Representing pit distribution in terms of identical spheres.

Following Eq. (3.4) and using the superposition principle of light waves, E_{track} is

$$E_{\text{track}}(\mathbf{q}) = E_{\text{sphere}} \sum_{l,m} c(l,m) e^{i\mathbf{q} \cdot \mathbf{p}(l,m)}, \quad l, m = 0, \pm 1, \pm 2 \dots \quad (3.7)$$

where E_{sphere} represents the common factor of the contributions of spheres, integers l and m are the indexes of a sphere, $c(l, m)$ is 1 (with pit) or 0 (without pit), and $\boldsymbol{\rho}(l, m)$ denotes the center location for a sphere at (l, m) . Referring to Fig. 4(b), $\boldsymbol{\rho}(l, m)$ can be further written as

$$\boldsymbol{\rho}(l, m) = \rho_x(l, m)\hat{\mathbf{x}} + \rho_y(l, m)\hat{\mathbf{y}}, \quad (3.8)$$

with

$$\begin{cases} \rho_x(l, m) = la + \delta_m \\ \rho_y(l, m) = mb \end{cases}, \quad l, m = 0, \pm 1, \pm 2, \dots \quad (3.9)$$

where δ_m represents the staggered shift for the first sphere in a track and is assumed *random* within $[-a/2, a/2]$. (Strictly speaking, δ_m is not random in the mathematical sense. However, considering that a cycle of a spiral track consists of a large number of various pit lengths and separations, the regularity of δ_m is almost completely lost.) Combining Eqs. (3.7), (3.8) and (3.9), we obtain

$$E_{\text{track}}(\mathbf{q}) = E_{\text{sphere}} \sum_m e^{imb\mathbf{q}\cdot\hat{\mathbf{y}} + i\delta_m\mathbf{q}\cdot\hat{\mathbf{x}}} \sum_l c(l, m) e^{ila\mathbf{q}\cdot\hat{\mathbf{x}}} \quad (3.10)$$

Now consider the case of perfect periodicity, that is, $c(l, m) = 1$ and $\delta_m = 0$. In this case, Eq. (3.10) reduces to

$$E_{\text{track}}(\mathbf{q}) = E_{\text{sphere}} \sum_m e^{imb\mathbf{q}\cdot\hat{\mathbf{y}}} \sum_l e^{ila\mathbf{q}\cdot\hat{\mathbf{x}}}, \quad (3.11)$$

and each summation generates a delta-function

$$\sum_l e^{ila\mathbf{q}\cdot\hat{\mathbf{x}}} = \delta[a\mathbf{q}\cdot\hat{\mathbf{x}} - 2\pi n], \quad n = 0, \pm 1, \pm 2, \dots \quad (3.12)$$

$$\sum_m e^{imb\mathbf{q}\cdot\hat{\mathbf{y}}} = \delta[b\mathbf{q}\cdot\hat{\mathbf{y}} - 2\pi n], \quad n = 0, \pm 1, \pm 2, \dots \quad (3.13)$$

These equations imply that the lights after diffraction appear only in discrete spatial directions for which the delta functions do not vanish. (This is similar to the X-ray diffraction pattern of crystal lattice [Kittel86].) Eq. (3.12) is equivalent to

$$a\mathbf{q}\cdot\hat{\mathbf{x}} - 2\pi n = 0, \quad n = 0, \pm 1, \pm 2, \dots \quad (3.14)$$

or

$$(\hat{\mathbf{k}}_1 - \hat{\mathbf{k}}_2) \cdot \hat{\mathbf{x}} = \frac{n\lambda}{a}, \quad n = 0, \pm 1, \pm 2, \dots \quad (3.15)$$

To study the real distribution of $c(l, m)$, let

$$f(\mathbf{q}, m) = \sum_l c(l, m) e^{ila\mathbf{q}\cdot\hat{\mathbf{x}}}. \quad (3.16)$$

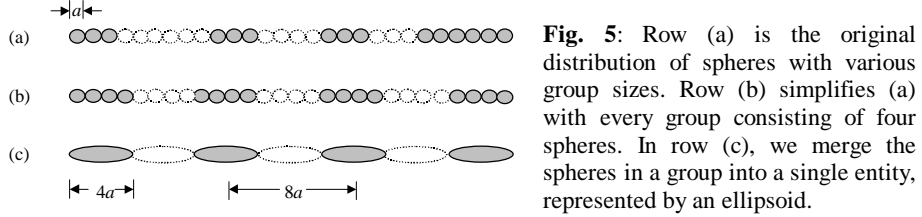
Although $c(l, m)$ takes 1 or 0 *randomly*, $f(\mathbf{q}, m)$ will still involve a delta function

$$f(\mathbf{q}, m) \approx \sum_l e^{ila\mathbf{q}\cdot\hat{\mathbf{x}}} = \delta[a\mathbf{q}\cdot\hat{\mathbf{x}} - 2\pi n], \quad n = 0, \pm 1, \pm 2, \dots \quad (3.17)$$

because the harmonics of different values of l tends to cancel with each other except for the constructive conditions specified by the delta function.

However, $c(l, m)$ should take on values 1 or 0 in *groups* of consecutive spheres.

Referring to Table 2, the pit lengths and separations are between 900 and 3300 nm and in steps of $a=300$ nm. To reflect this distribution effectively, we simplify the distribution by modeling pits using uniform groups, as shown in Fig. 5. In the simplified representation, every group consists of four spheres because the average lengths of pit grooves is $4a$ (see the Appendix).



Thus $f(\mathbf{q}, m)$ can be written as

$$f(\mathbf{q}, m) = f(\mathbf{q}) \approx C_{\text{ellip}} \sum_l e^{il(8a)\mathbf{q} \cdot \hat{\mathbf{x}}} = C_{\text{ellip}} \delta[8a(\mathbf{q} \cdot \hat{\mathbf{x}}) - 2\pi l], \quad (3.18)$$

where C_{ellip} represents the common factor for the contributions of ellipsoids (or groups of spheres) and $8a$ is the periodic spacing between solid ellipsoids. Since this result is independent of m , we can write $f(\mathbf{q}, m)$ as $f(\mathbf{q})$. The first two minor strips on both sides of the major strip correspond to $n = \pm 1$

$$8a(\mathbf{q} \cdot \hat{\mathbf{x}}) \pm 2\pi = 0 \quad (3.19)$$

or

$$(\hat{\mathbf{k}}_1 - \hat{\mathbf{k}}_2) \cdot \hat{\mathbf{x}} = \pm \frac{\lambda}{8a} \quad (3.20)$$

Thus a light with larger λ will have a larger value of $|(\hat{\mathbf{k}}_1 - \hat{\mathbf{k}}_2) \cdot \hat{\mathbf{x}}|$. Recalling that the location of the major strip is given by the condition $(\hat{\mathbf{k}}_1 - \hat{\mathbf{k}}_2) \cdot \hat{\mathbf{x}} = 0$, the larger value of $|(\hat{\mathbf{k}}_1 - \hat{\mathbf{k}}_2) \cdot \hat{\mathbf{x}}|$ implies that the red components of the minor strips are farther from the major strip while the blue components are closer. This explains the color change in minor strips.

Combining Eqs. (3.1), (3.10) and (3.16), we have

$$I(\mathbf{q}) \propto |E_{\text{track}}(\mathbf{q})|^2 \propto |g(\mathbf{q})|^2 \cdot |f(\mathbf{q})|^2, \quad (3.21)$$

where we define

$$g(\mathbf{q}) = \sum_m e^{imb\mathbf{q} \cdot \hat{\mathbf{y}} + i\delta_m \mathbf{q} \cdot \hat{\mathbf{x}}}. \quad (3.22)$$

3.2 Non-Diffractive Contribution

The appearance of an optical disk also relies on a non-diffractive factor. Fig. 6 shows a photograph of a vinyl record with a CD-ROM placed on top of it. Note that the bright strip on the vinyl record aligns with that on the CD-ROM. Because there is no diffraction on the vinyl record, the bright strip on the vinyl record must be caused by some non-diffractive mechanism, which should also apply to a CD-ROM as well.



Fig. 6: Photograph of a vinyl record with a CD-ROM on the top shows the aligned bright strips due to the non-diffractive effect.

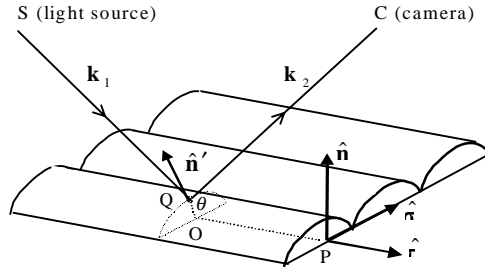


Fig. 7: Reflection on a cylindrically grooved surface.

The concentric tracks can be characterized as parallel cylindrical surfaces as shown in Fig. 7. (We describe the surface details with raised cylindrical surfaces although concentric tracks of optical disks are in fact concave – this is just for clarity of illustration and will not affect the derived result.) We claim that *the necessary and sufficient condition for generating a bright strip on a surface with such a parallel cylindrical structure is*

$$(\hat{\mathbf{k}}_2 - \hat{\mathbf{k}}_1) \cdot \hat{\boldsymbol{\tau}} = 0, \quad (3.23)$$

where $\hat{\boldsymbol{\tau}}$ is the longitudinal direction for the cylindrical surfaces oriented in parallel, and $\hat{\mathbf{k}}_1$ and $\hat{\mathbf{k}}_2$ are the incident and reflective directions. To prove sufficiency, we must show that if $\hat{\mathbf{k}}_1$ and $\hat{\mathbf{k}}_2$ satisfy Eq. (3.23) then the received light is a highlight. To do so, we only need to show that there exists a small neighborhood area (but still containing many cylindrical surface pieces) for the illuminated point P such that the local surface normal direction $\hat{\mathbf{n}}'$ (primed) at a point Q within the neighborhood area is parallel to the midway vector $\hat{\mathbf{k}}_2 - \hat{\mathbf{k}}_1$ for the reflection. According to Eq. (3.23), $\hat{\mathbf{k}}_2 - \hat{\mathbf{k}}_1$ has no component along the $\hat{\boldsymbol{\tau}}$ direction and therefore it can be written as

$$\hat{\mathbf{k}}_2 - \hat{\mathbf{k}}_1 = \hat{\boldsymbol{\sigma}} \cos \theta + \hat{\mathbf{n}} \sin \theta. \quad (3.24)$$

At point Q with the same polar angle θ , the local surface normal direction $\hat{\mathbf{n}}'$ will be parallel to $\hat{\mathbf{k}}_2 - \hat{\mathbf{k}}_1$. Thus we have proved sufficiency. To show necessity, suppose that we have a bright strip. Then there exists a point Q in the neighborhood area such that at this point the perfect specular reflection holds. In other words, $\hat{\mathbf{k}}_1 - \hat{\mathbf{k}}_2$ is parallel to the surface normal direction $\hat{\mathbf{n}}'$ at point Q. Since $\hat{\mathbf{n}}'$ is on the plane formed by $\hat{\boldsymbol{\sigma}}$ and $\hat{\mathbf{n}}$, so is $\hat{\mathbf{k}}_2 - \hat{\mathbf{k}}_1$. Thus Eq. (3.23) holds.

In practical computations, it is necessary to express the condition (3.23) through a smooth peak function. Similar to the idea of the Phong model [Phong75], we replace Eq. (3.23) by making reflected light intensity behave as

$$I \propto |(\hat{\mathbf{k}}_1 - \hat{\mathbf{k}}_2) \cdot \hat{\boldsymbol{\tau}}|^\beta, \quad (3.25)$$

where β is a positive integer. This equation can be regarded as an extension of the Phong model to anisotropic surfaces. Note that at the macroscopic scale, the groove direction $\hat{\boldsymbol{\tau}}$ depends on the surface location. For an optical disk, $\hat{\boldsymbol{\tau}}$ is along the

tangent direction of concentric tracks.

Here we should mention previous work of Poulin and Fournier [Poulin90] on modeling anisotropic surfaces. Poulin and Fournier considered more details of anisotropic surfaces including the presence of flat lands and the dimensions of the structures. Their work is useful for evaluating the accuracy of Eq. (3.25) and determining parameter β for specific anisotropic surfaces.

3.3 Combined Illumination Equations

Combining the results of the previous subsections, we write the total intensity of reflected light from the surface of an optical disk as

$$\begin{aligned} I_{\text{total}}(\mathbf{k}_1, \mathbf{k}_2) &= I_{\text{non-diff}}(\mathbf{k}_1, \mathbf{k}_2) + I_{\text{diff}}(\mathbf{k}_1, \mathbf{k}_2) \\ &= I_{\text{non-diff}}(\mathbf{k}_1, \mathbf{k}_2) + c_0 |(\hat{\mathbf{k}}_1 - \hat{\mathbf{k}}_2) \cdot \hat{\boldsymbol{\tau}}|^\beta \cdot |g(\mathbf{q})|^2 \cdot |f(\mathbf{q})|^2, \end{aligned} \quad (3.26)$$

where c_0 is a positive constant, $\hat{\boldsymbol{\tau}}$ is the track direction at the illuminated point, and $\mathbf{q} = \mathbf{k}_1 - \mathbf{k}_2$. It is often useful to rewrite this equation in the following form

$$I_{\text{total}}(\mathbf{k}_1, \mathbf{k}_2) = I_0(\lambda)[R_{\text{non-diff}}(\mathbf{k}_1, \mathbf{k}_2) + R_{\text{diff}}(\mathbf{k}_1, \mathbf{k}_2)], \quad (3.27)$$

where $I_0(\lambda)$ is the incident intensity, and $R_{\text{diff}}(\mathbf{k}_1, \mathbf{k}_2)$ and $R_{\text{non-diff}}(\mathbf{k}_1, \mathbf{k}_2)$ are

$$R_{\text{diff}}(\mathbf{k}_1, \mathbf{k}_2) = c_0 |(\hat{\mathbf{k}}_1 - \hat{\mathbf{k}}_2) \cdot \hat{\boldsymbol{\tau}}|^\beta \cdot |g(\mathbf{q})|^2 \cdot |f(\mathbf{q})|^2 \quad (3.28)$$

and

$$R_{\text{non-diff}}(\mathbf{k}_1, \mathbf{k}_2) = c_{\text{diffuse}} \cdot (\hat{\mathbf{k}}_2 \cdot \hat{\mathbf{n}}) + c_{\text{specular}} \cdot |\hat{\mathbf{q}} \cdot \hat{\mathbf{n}}|^\alpha, \quad (3.29)$$

where $\hat{\mathbf{n}}$ the disk surface normal. Furthermore, we can use delta-functions to approximate $|f(\mathbf{q})|^2$ and $|g(\mathbf{q})|^2$

$$|f(\mathbf{q})|^2 \approx c_1 \sum_{n=-\infty}^{\infty} \delta[8a \cdot (\mathbf{q} \cdot \hat{\boldsymbol{\tau}}) - 2\pi n] + c_2, \quad (3.30)$$

and

$$|g(\mathbf{q})|^2 \approx c_3 \sum_{n=-\infty}^{\infty} \delta[b \cdot (\mathbf{q} \cdot \hat{\boldsymbol{\sigma}}) - 2\pi n] + c_4, \quad (3.31)$$

where c_1 , c_2 , c_3 , and c_4 are positive constants. For a more precise description we should let the peaks have finite widths. This can be done by replacing every delta-function with a Gaussian function of the form

$$p(t, t_0) = \frac{\sqrt{\pi}}{2w} e^{-4(t-t_0)^2/w^2} \quad (3.32)$$

where t_0 and w represent the center and width of the peak. The purpose of the factor in front of the exponential is to normalize the Gaussian. Thus $|f(\mathbf{q})|^2$ can be modeled by a multiple-peak function as

$$|f(\mathbf{q})|^2 = h(t) = c_1 \sum_{n=-\infty}^{\infty} p(t, 2\pi n) + c_2 = \frac{c_1 \sqrt{\pi}}{2w} \sum_{n=-\infty}^{\infty} e^{-4[8a \cdot (\mathbf{q} \cdot \hat{\boldsymbol{\tau}}) - 2\pi n]^2/w^2} + c_2, \quad (3.33)$$

where $t = 8a \cdot (\mathbf{q} \cdot \hat{\boldsymbol{\tau}})$. Similarly we can model $|g(\mathbf{q})|^2$. Fig. 8 shows the profiles of the multiple-peak function $h(t)$ in the range $[0, 4\pi]$ with fixed c_1 and c_2 , and

various peak widths w .

Finally, we have some general comments. First, c_2 and c_4 will be zero if the disk surface structure is perfectly periodic. However, they should be positive constants because pits are *partially* periodic. The periodicity imperfection results in scattering in all spatial directions, which effect is included in the diffuse term in Eq. (3.29). In the case that the surface structure is completely random and the surface is regarded as entirely diffuse, all the delta-function terms vanish. Second, to conserve energy, we should relate constants c_1 and c_2 as well as c_3 and c_4 so that the profiles shown in Fig. 8 maintain the same underneath areas. Also, our model obeys the reciprocity principle because, if we switch the incident and reflected directions, the result due to diffraction according to Eq. (3.28) is the same, that is, $R_{\text{diff}}(-\mathbf{k}_2, -\mathbf{k}_1) = R_{\text{diff}}(\mathbf{k}_1, \mathbf{k}_2)$. Finally, in this paper we will focus on *relative* light intensity distributions because calculating the absolute values of light intensities involves more low-level physical information such as exact pit shapes, which deviates too much from our main interest – generating iridescent strips of optical disks. Thus in rendering, we will adjust the relevant intensity constants to obtain the appropriate visual effect (including proper relative intensities among the major strip, minor strips and the rest area). But in principle it is possible to determine these intensity constants from low-level physical information such as the percentage area covered by pit grooves, exact pit shapes etc.

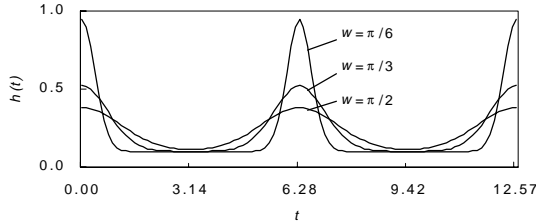


Fig. 8: Profiles of multiple peaks with different peak widths $w = \pi/6, \pi/3, \pi/2$.

4 Rendering

Although diffraction involves phases of light waves, Eqs. (3.27)-(3.29) show that it can be rendered based on *spectral* information. The rendering process can be divided into three stages. First, we generate a *spectral image* using the spectral information based on local and global illumination models. A spectral image is similar to a color image except that for every pixel the information is a spectral power distribution instead of a color. In our rendering, we use Eqs. (3.27)-(3.29) for local illumination and ray tracing for global illumination. A ray tracer provides all the required information for our illumination model, including the illuminating and viewing directions and the illuminated point. Hence we need simply follow the standard raytracing procedure (cf. p780 in [Foley96]) except that we must shade according to Eqs. (3.27)-(3.29) if the intersected point is in the data region of an optical disk. In the second stage, we transform the spectral image into a generic color image described with colors in the CIE XYZ model. In the last stage, we derive the final RGB image by clipping the CIE XYZ colors into an RGB gamut. The RGB gamut can be chosen

differently and various algorithms are available for the color clipping [Hall89]. We will use the simplest algorithm: whenever an RGB component derived from a CIE XYZ color is above 1 or below 0, we reset the value to 1 or 0, respectively. This method however may result in shift of hue. This can be improved by other clipping methods such as desaturation or uniform downscaling of colors outside the gamut.

Spectral representation is a critical question. Although sampling is commonly used, it does not work well for computing light diffraction. As shown above, light diffraction inherently involves delta functions that generate sharp peaks. To accurately describe a sharp peak with the sampling method, we have to use *many* sampling points, which is disadvantageous in both memory and performance. Our approach is to represent all spectra with the *composite model* [Sun98]. Its basic idea is to decompose a spectral function into its *smooth background* and a collection of *spikes*. The smooth component can be represented through sampling while a spike can be simply described through its location and weight (or height). It is straightforward to implement the samples of the smooth background with an array and spectral spikes with a linked list. (Usually the accuracy is sufficient if we use 10 sampling points for the smooth background [Sun98].) This model is accurate, compact and efficient, and is flexible to add or manipulate spikes created dynamically by light diffraction. Fig. 9 describes how to handle related spikes. Note that when two light rays overlap and their intensities contain spikes at same or very close wavelengths, the spikes will be merged into a single one. This prevents spike proliferation as well as optimizes the representation with respect to compactness and performance.

```

double temp = b * fabs( // "fabs" is for absolute value
    (unitVector_k1 - unitVector_k2) * diskRadianDir ); // dot product
int n = 1; // initialize n for the first-order construction
double spike_wl = temp / n; // spike wavelength

while (spike_wl > 400) // if spike_wl below 400, no contributions
{
    if (spike_wl < 700) // spike_wl in visible range
    {
        get incident_SPD at spike_wl; // incident_SPD is known from input
        compute f_square at spike_wl; // |f|^2 at spike_wl
        compute pitShapeFactor; // according to Eq (3.25)
        double spike_value = incident_SPD * f_square * pitShapeFactor; // Eq (3.28)
        Cspike spike(spike_wl, spike_value); // create a new spike instance
        add spike to the reflective intensity
    }
    n++; // next order construction
    spike_wl = temp / n; // new spike wavelength
}

```

Fig. 9: Pseudocode for adding contributions of delta-functions as spikes.

Color Plate 1 displays two photographs of a CD-ROM and the corresponding rendered images, which match the photographs very well including the colors and orientations of the major and minor strips. Here, one may note that Eqs. (3.12), (3.13) and (3.23) are three conditions on three parameters (namely the wavelength and two parameters for location) and therefore we should observe single monochromatic highlights instead of strips. However, Eq. (3.23) corresponds to the case of $n=0$ of Eq. (3.12) and is thus not an independent condition.

An important characteristic in the appearance of an optical disk is its sensitive

dependency on the illuminating and viewing directions. Color Plate 2 shows a series of rendered images for different illuminating angles with the camera fixed (an animation is available at the URL ???). The point light source moves up along the z -axis and the eight images correspond to different heights of the light source.

Color Plate 3 shows a rendered optical disk under illumination of *three* point light sources with similar illumination directions. The result looks more like what we observe in reality, as a source always has a finite surface. This image shows the possibility of using a cluster of point sources to represent a *surface* light source.

The rendered image in Color Plate 4 demonstrates an interesting interaction between a CD-ROM and a plastic sphere. We can clearly recognize the major and minor strips of the reflected image of the CD-ROM on the sphere, except that the strips are curved due to the spherical surface. Note that the strip colors shown on the sphere are different from those shown on the CD-ROM itself because the viewing directions relative to the CD-ROM for the two cases are different. This shows that our illumination model also works well in multiple-object environments.

5 Future Directions and Conclusion

The core idea of our diffractive illumination model, i.e. deriving the light intensity distribution based on structural periodicity and the superposition principle of light waves, would work equally well for other diffractive structures. For instance, it also applies to artificially structured textures of metallic coatings used in decorations, stickers, or artwork. Films of certain types of liquid crystals contain layer gratings and can cause both reflected and transmitted diffraction [Nassau83], and our model also applies to such films. Notably, some of the most outstanding colors on natural objects are associated with light diffraction, often along with interference [Williamson83, Nassau83]. For example, the iridescent colors of mother-of-pearl are attributed to a combination of diffraction and interference. Another example is the spectacular colors of a gemstone opal, often called “opalescence”. In particular, the surface of certain beetles and wasps has a hard corrugation arranged in closely spaced rows, which can cause significant diffraction (see page 111 and plate 16 in [Williamson83]).

In conclusion, we have proposed an illumination model to handle light diffraction at the microstructure of optical disks. This model is based on the physical structure of optical disks and the superposition principle of light waves. The calculations are straightforward, analytic, and self-contained. We have also discussed the non-diffractive factor due to surface anisotropy and have derived the general condition for surface highlights. In spite that our modeling process involves light wave phases, the final result of our model can be completely described in terms of spectra. This allows us to render diffraction based on spectra, which can be effectively represented with a composite model proposed in our early work. The images that we rendered with a ray tracer have excellent agreement with their corresponding photograph counterparts and have achieved good realism in general.

Appendix

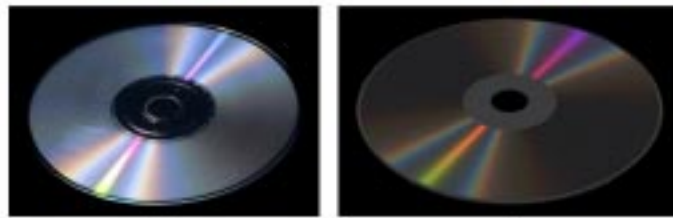
Here we prove that the average length of pit grooves is $4a$. Randomly we pick a pit groove. Since the minimum length is $3a$ [Noldeke90], the probability for this groove being $3a$ long (i.e. the fourth sphere being empty in Fig. 4) is 0.5 because of the equal probabilities for the fourth sphere to be solid and empty. Similarly, the probability for

this groove being $4a$ long is 0.5×0.5 , the probability for the fourth sphere being solid times the probability for the fifth sphere being empty. The same analysis works for all longer lengths. Thus, the average length is the sum of pit lengths times probabilities

$$\bar{l} = \sum_{k=3}^{\infty} k \cdot \frac{1}{2^{k-2}} = \sum_{k=1}^{\infty} \frac{k+2}{2^k} = \sum_{k=1}^{\infty} \frac{k}{2^k} + 2 \sum_{k=1}^{\infty} \frac{1}{2^k} = 2 + 2 = 4.$$

References

- Beckmann63 P. Beckmann and A. Spizzichino, *The Scattering of Electromagnetic Waves from Rough Surfaces*, Macmillan, New York, 1963.
- Born75 M. Born and E. Wolf, *Principles of Optics: Electromagnetic Theory of Propagation, Interference and Diffraction of Light*, Pergamon, Oxford, 1975.
- Foley96 J. D. Foley, A. van Dam, S. K. Feiner, and J. F. Hughes, *Computer Graphics Principles and Practice*, Second Edition, Assison-Wesley, Reading, MA, 1996.
- Hall89 R. A. Hall, *Illumination and Color in Computer Generated Imagery*, Springer-Verlag, New York, 1989.
- He91 X. D. He, K. E. Torrance, F. X. Sillion, and D. P. Greenberg, "A Comprehensive Physical Model for Light Reflection," *Computer Graphics, Proc. of ACM SIGGRAPH 91*, ACM Press, New York, 1991, pp. 175-186.
- Hecht98 E. Hecht, *Optics*, Third Edition, Addison-Wesley, Reading, MA, 1998.
- Kittel86 C. Kittel, *Introduction to Solid State Physics*, 5th Edition, John Wiley & Sons, New York, 1986.
- Nassau83 K. Nassau, *The Physics and Chemistry of Color: The Fifteen Causes of Color*, John Wiley & Sons, New York, 1983.
- Noldeke90 C. Noldeke, "Compact Disc Diffraction," *The Physics Teacher*, Oct. 1990, pp. 484-485.
- Phong75 B. Phong, "Illumination for Computer Generated Images," *Communications of the ACM*, Vol. 18, No. 6, 1975, pp. 311-317.
- Poulin90 P. Poulin and A. Fournier, "A Model for Anisotropic Reflection," *Computer Graphics, Proc. of ACM SIGGRAPH 90*, ACM Press, New York, 1990, pp. 273-282.
- Purcell97 L. Purcell and D. Martin, *The Complete Recordable-CD Guide*, Sybex, San Francisco, 1997.
- Schwartz93 K. Schwartz, *The Physics of Optical Recording*, Springer-Verlag, Berlin, 1993.
- Stam99 J. Stam, "Diffraction Shaders," *Computer Graphics, Proc. of ACM SIGGRAPH 99*, ACM Press, New York, 1999, pp. 101-110.
- Sun98 Y. Sun, F. D. Fracchia, and M. S. Drew, "A Composite Model for Representing Spectral Functions," *Simon Fraser University, Technical Report SFU CMPT TR 1998-18*, 1998. Available at <ftp://fas.sfu.ca/pub/cs/TR/1998/>.
- Sun99 Y. Sun, F. D. Fracchia, M. S. Drew, and T. W. Calvert, "Rendering Iridescent Colors of Optical Disks," *Simon Fraser University, Technical Report SFU CMPT TR 1999-08*, (1999). Available at <ftp://fas.sfu.ca/pub/cs/TR/1999/>.
- Williamson83 S. J. Williamson and H. Z. Cummins, *Light and Color in Nature and Art*, John Wiley and Sons, New York, 1983.



a

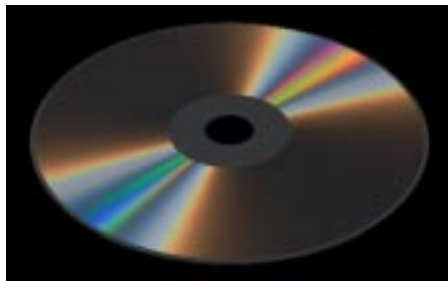
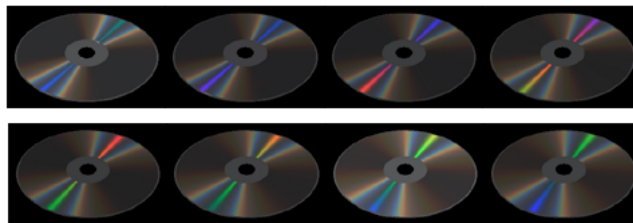
b



c



d



- 1
- 2
- 3
- 4

1 (a) and (c) are photographs of a CD-ROM for different illuminating and viewing directions, and (b) and (d) are the rendered images corresponding to (a) and (c). 2 The rendered images for a point light source with different illuminating angles. 3 A rendered CD-ROM under illumination of three point light sources. 4 Interaction between a CD-ROM and a white plastic sphere.